



# 3D finite element analysis of slot milling of unidirectional glass fiber reinforced polymer composites

C. Prakash<sup>1</sup> · K. S. Vijay Sekar<sup>2</sup>

Received: 4 October 2017 / Accepted: 16 April 2018 / Published online: 7 May 2018  
© The Brazilian Society of Mechanical Sciences and Engineering 2018

## Abstract

The applications of glass fiber reinforced polymer composite materials are increasing in many industries, such as automobile, aerospace, construction, marine, and defense. The slot milling is an important machining operation to reduce the excess material and to bring the component to the required final shape and size. However, machining the glass fiber reinforced polymer composite laminate is still challenging due to its non-homogeneity and anisotropic properties. In this research, 3D finite element model is developed using ABAQUS/explicit to investigate the cutting forces, chip formation process, and the laminate failure modes. The material model is created using Autodesk HELIUS PFA and the 3D Hashin's criteria are incorporated to characterize the failure modes. The finite element model effectively analyzes the interaction between tool and laminate, to evaluate the possible failure modes of the GFRP laminate, effects of cutting forces for different cutting speeds, and feed rates during the slot milling process. Moreover, the finite element simulation results are validated by comparing with the experimental results and the literature. From the investigation, it is found that the effect of cutting speed and feed rate involves more in the chip characteristics, which is confirmed with the scanning electron microscope images of the milled chips. The chips obtained are mostly discontinuous fractured chips in powder form with fiber pullout and delaminated fibers.

**Keywords** GFRP · Slot milling · Cutting forces · Chip formation · SEM · 3D finite element model

## 1 Introduction

Glass fiber reinforced polymer (GFRP) composite materials have found wide applications as functional and structural materials due to its static, dynamic, thermal, and chemical properties. They provides high specific strength/stiffness, low density, long fatigue life, strength-to-weight ratio, superior corrosion resistance, light weight construction, high damping, low thermal conductivity, high fatigue strength, and resistance to chemical and microbiological

attacks [1–3]. These superior properties and the potential applications, nowadays, create the interest for the researchers and need to understand the machining process of the GFRP laminate.

GFRP composite laminates are made to near-net shape, but simple conventional machining operations are essential to assemble and to integrate with other components of the system. However, the non-homogeneity, anisotropic, and abrasive nature of the composite causes different kinds of problems during these machining operations such as milling and drilling [4]. The common defects associated in machining of GFRP laminates are micro-cracking, fiber breakage, fiber pull-out, matrix cracking, and delamination. Moreover, the delamination is found to be one of the major defects, which influences more in the chip formation during the slot milling operation of GFRP composite [5–7].

The experimental study is very much-needed to overcome these machining difficulties. Hence, the researchers concentrate more on these studies to understand the complex slot milling process. However, it is time-consuming and very expensive, especially during a wider

---

Technical Editor: Márcio Bacci da Silva.

✉ C. Prakash  
prakashc@suryagroup.edu.in

<sup>1</sup> Department of Automobile Engineering, School of Engineering and Technology, Surya Group of Institutions, Villupuram District, Vikiravandi, Tamilnadu 605652, India

<sup>2</sup> Department of Mechanical Engineering, SSN College of Engineering, Kancheepuram District, Kalavakkam, Tamilnadu 603110, India

machinability metric (i.e., variation in tool geometry, materials, and cutting conditions) is considered [4, 8, 19]. In addition to this, experimenting and interpreting the results mainly depend upon the accuracy of the machineries and calibration of the equipments used. Hence, finite element method is preferred to overcome these difficulties and to simulate and understand the complex chip formation process.

AZMI, A.I [9] conducted experimental studies to understand the chip formation process during end milling of glass fiber reinforced polymer composites. He reported that the chips produced are discontinuous, fracturing, and shattered powdery particles. Moreover, the collected chip reveals the various modes of failures, such as bending, buckling, fracture, delamination, and crushing—compression of fiber and matrix material.

Lasri et al. investigated the machining of GFRP using FE model with maximum stress and Hashin criterion. The objective of this study is to better understand the chip formation process and to analyze the cutting-induced damage from initiation stage until complete chip formation. The cutting forces predicted using Hashin Failure criterion are close to the experimental results [10].

Seyedbehzad Ghafarizadeh et al. developed 2D FE model to investigate the chip formation, machining damage, and cutting forces during the milling operation in CFRP. The FE results are in good agreement with the experimental results. Moreover, they concluded that the machining damage mainly depends upon fiber orientation, fiber compression damage, and matrix cracking [6].

He et al. developed macro- and micro-FE models of milling of CFRP using ABAQUS. Three-dimensional Hashin criteria are used for material damage prediction. The simulation results shows that the cutting forces  $F_x$  and  $F_y$  in the macro model are very close in correlation with the experimental results. The results also show that both the milling forces and delamination increase with the increasing feed rate and decrease with the increasing spindle speed [11].

Oğuz Çolak et al. investigated the effects of cutting forces and surface quality in milling the CFRP laminate under different cutting conditions. Their conclusions are as follows: cutting forces are minimum at higher cutting speed and lower feed rate. Moreover, surface roughness increases with increasing feed rate and decreasing cutting speed [5].

The developed and validated 3D finite element model is a boon to the industries and researchers to study the complex cutting mechanisms in milling the GFRP laminates [20].

From the literature and to the authors knowledge, although many FE models have been proposed for the simulation of milling and drilling, 3D finite element model

is not yet developed for the slot milling operation particularly for GFRP laminate, since it requires huge computation time. In GFRP composites, fiber pullout and delamination damages are very predominant during milling operation [7, 9]. However, 3D FE model is only capable of predicting the chip formation process and the delamination damages very effectively when compared to 2D model [12].

Thus, a 3D FE model is developed in ABAQUS/Explicit to predict the cutting forces, chip formation process, chip characteristics, modes of failure of the laminate, working stress, and fiber–matrix failure. Furthermore, to validate the developed 3D FE model, milling experiments were conducted on unidirectional fiber reinforced GFRP (UD-GFRP) laminate and compared with the FE simulation results. The influence of the cutting parameters over the chip formation is investigated using the chip photographs and scanning electron microscope (SEM) images.

The proposed 3D FE model benefits the manufacturing industries in the following ways: it helps to reduce the number of experimental trials required to optimize the machining process. The predicted values can be extrapolated to analyze the machining behavior even in very high cutting conditions. The industry is reeling from higher material procurement and processing cost due to the experimental work, and such predictive numerical methods alleviate the cost and provide better solutions in quick time.

## 2 Experimental setup

The milling experiments were conducted on a NAMMIL XL6026AV vertical milling machine. This machine has the maximum spindle power of 2 HP and a maximum spindle speed of 1700 rpm. Solid carbide TiAlN coated four fluted-end mill cutter with the 10 mm diameter, which is preferred [11, 13] for performing the slot milling operation. The slot milling was performed (as shown in Fig. 1) for various machining parameters, as shown in Table 1.

The literature depicts that the higher cutting speeds and feed rates produce improper chip formation. The chips are mainly dust of micro-sized particles, when the spindle speed is greater than 1000 rpm [6, 7, 9]. Hence, the machining parameters were minimised for experimental study, with spindle speed < 1000 rpm and feed rate < 200 mm/min, which facilitate to investigate on chip characteristics and the damage modes of the laminate very effectively. The four-channel IEICOS dynamometer (Model number 6306) was used to capture the cutting force data (shown in Fig. 1c). The cutting force data mentioned in Table 2 were obtained from the experimental study, which matches with the literature [7, 9, 10] and with the 3D FE simulation results.

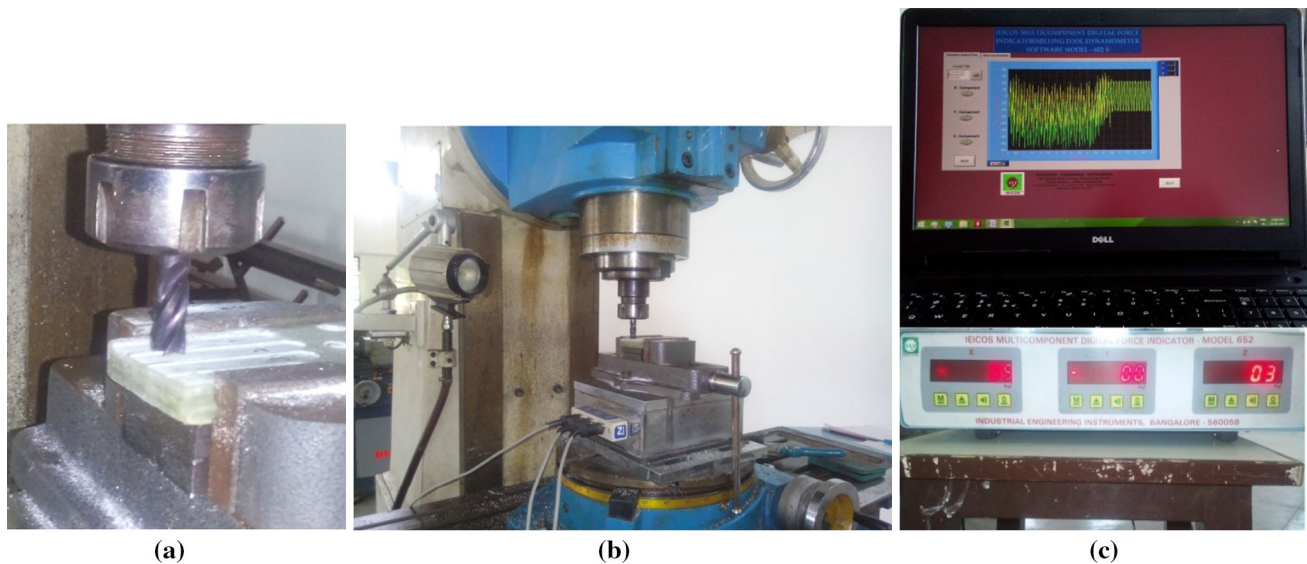


**Fig. 1** a Work and tool. b Experimental setup. c Data acquisition system

**Table 1** Machining parameters used in milling of GFRP laminate

Milling parameters	Magnitude
Spindle speeds, $N$ (rpm)	350, 660, 900, 1700
Cutting speed, $V_c$ (m/min)	10.99, 18.84, 28.26, 53.38
Feed rate, $f$ (mm/min)	50, 150
Depth of cut (mm)	1
Fiber orientation	0° unidirectional

The cutting force data obtained from experimental result reveal, at lower cutting speed and feed, the cutting forces are maximum. However, at higher cutting speeds and feed, the cutting forces are reduced by 40–50% as shown in Table 2.

**Table 2** Experimental results of average cutting force at different cutting speeds and feed rates

Feed rate, $f$ (mm/min)	Cutting speed, $V_c$ (m/min)	Max. cutting force, $F_x$ (N)	Max. cutting force, $F_y$ (N)	Max. cutting force, $F_z$ (N)
50	10.99	42	31	15
	18.84	28	24	11
	28.26	19	21	12
	53.38	17	15	10
150	10.99	28	24	10
	18.84	19	20	9
	28.26	21	19	11
	53.38	18	15	10

### 3 Finite element model

#### 3.1 Methodology

In this research work, 3D finite element model is developed using the commercially available FEA software (ABAQUS/Explicit 6.14-2) to simulate the slot milling process in the unidirectional GFRP laminate. ABAQUS/explicit does not have built in 3D Hashin damage criteria [8, 14, 15]. Hence, AUTODESK HELIUS PFA plug-in is used to incorporate the material properties of the laminate, damage initiation, and damage evolution criteria. The FE model is developed to accurately characterize the dynamic characteristics of the slot milling process, considering the complex end mill cutter geometry and interaction properties between the tool and the work piece.

**Table 3** Properties and Geometric Specifications of Carbide Drill Bit

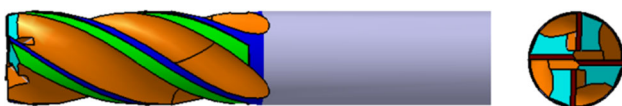
Specifications/description	Value(s)
Product	Twist drill
Shank type	Plain
Drill diameter (mm)	10
Overall length (mm)	62.50
Shank length (mm)	32.50
Flute length (mm)	30
Shank diameter (mm)	10
Material	Solid carbide
Type	High-performance drill
Number of flutes	02
Drill style	Metric
Coating	TiAlN
Coating thickness	2–5 $\mu\text{m}$
Working temperature	Max 900 $^{\circ}\text{C}$
Coating colour	Reddish, violet, black
Hardness	3300 Hv
Density (kg/m <sup>3</sup> )	11,560
Helix angle ( $^{\circ}$ )	30
Point angle ( $^{\circ}$ )	130
Chisel edge radius (mm)	0.7
Chisel edge angle ( $^{\circ}$ )	135
Lip relief angle ( $^{\circ}$ )	12

### 3.2 Geometric model of the tool and workpiece

A 3D homogeneous UD-GFRP workpiece model is created using ABAQUS—part module with the dimensions 25 mm  $\times$  25 mm  $\times$  3 mm, as shown in Fig. 8, 9. Solid carbide end mill cutter (SANDVIK H10F Grade with 115 $^{\circ}$  point angle; 30 $^{\circ}$  helix angle with 4 Flutes) of diameter 10 mm was modeled in CATIA V5R14 [16] (as shown in Fig. 2). This 3D part model is then imported to ABAQUS as a rigid body in Interactive Graphic Exchange System (IGES) file format. The Properties and Geometric Specifications of Carbide Drill Bit are given in Table 3.

### 3.3 3D finite element model

The FE model consists of a UD-GFRP laminate with the average element size of 0.25 mm and 50,000 elements meshed with C3D8R (linear 8-node linear brick, reduced integration, and hourglass control). The end mill cutter model is considered to be a rigid body [14], which consists

**Fig. 2** 3D Model of four fluted-end mill cutter**Table 4** Finite element model—input data

Work piece	UD-GFRP laminate
Tool	Dia. 10 mm
Dimensions of FE model	25 $\times$ 25 $\times$ 10 mm
Type of element in work piece	C3D8R
Number of elements in work piece	50,000
Number of nodes in work piece	54,621
Element size in workpiece	0.25 mm
Type of element in tool	C3D10 M
Number of elements in tool	32,895
Number of nodes in tool	49,665
Element size in tool	1 mm
Total elements and nodes in FE model	82,895 and 104,286
Friction factor	0.7
Failure criteria	3D HASHIN

Refer Table 1

of 32,895 elements meshed with C3D10 M (10-node modified quadratic tetrahedron), and the element size is around 1 mm (refer Table 4; Figs. 8, 9).

### 3.4 Constitutive material modeling

The GFRP laminate used for this FE simulation is a uni-directional laminate with 65% fiber content and it is considered to be an orthotropic homogeneous material. The UD-GFRP laminate is made of TAIRYFIL glass fiber and epoxy adhesive. The mechanical properties of the GFRP laminate are given in Table 5.

**Table 5** Mechanical properties of GFRP laminate

Specifications	Value(s)
Longitudinal modulus, $E_x$ (GPA)	40
Transverse modulus, $E_y$ (GPA)	8
Transverse modulus, $E_z$ (GPA)	8
Shear modulus in 1–2 plane, $G_{xy}$ (GPA)	4
Shear modulus in 2–3 plane, $G_{yz}$ (GPA)	3
Shear modulus in 1–3 plane, $G_{xz}$ (GPA)	4
Poisson's ratio, $\nu$	0.25
Density (kg/m <sup>3</sup> )	1992
Specific gravity	1.99
Longitudinal tensile strength, $X_t$ (MPa)	1000
Longitudinal comp. strength, $X_c$ (MPa)	600
Transverse tensile strength, $Y_t$ (MPa)	30
Transverse comp. strength, $Y_c$ (MPa)	110
Shear strength in 1–2 plane, $S_{xy}$ (MPa)	40
Shear strength in 2–3 plane, $S_{yz}$ (MPa)	40
Shear strength in 1–3 plane, $S_{xz}$ (MPa)	40
Resin/fiber ratio	35:65 [ $\pm$ 5]
Fiber orientation	0

The 3D Hashin failure criteria with related constitutive model are incorporated into ABAQUS/explicit using a VUMAT subroutine provided by AUTODESK HELIUS PFA plug-in for the 3D solid elements [14, 15].

The GFRP laminate is modeled as a homogeneous orthotropic elastic material before the damage initiation.

The stress–strain relationship is given by the following:

$$\begin{Bmatrix} \sigma_x \\ \sigma_y \\ \sigma_z \\ \tau_{xy} \\ \tau_{yz} \\ \tau_{xz} \end{Bmatrix} = \begin{bmatrix} C_{11}^0 & C_{12}^0 & C_{13}^0 & 0 & 0 & 0 \\ C_{12}^0 & C_{22}^0 & C_{23}^0 & 0 & 0 & 0 \\ C_{13}^0 & C_{23}^0 & C_{33}^0 & 0 & 0 & 0 \\ 0 & 0 & 0 & C_{44}^0 & 0 & 0 \\ 0 & 0 & 0 & 0 & C_{55}^0 & 0 \\ 0 & 0 & 0 & 0 & 0 & C_{66}^0 \end{bmatrix} \begin{Bmatrix} \epsilon_x \\ \epsilon_y \\ \epsilon_z \\ \gamma_{xy} \\ \gamma_{yz} \\ \gamma_{xz} \end{Bmatrix}, \tag{1}$$

where

$$C_{11}^0 = E_x(1 - \nu_{yz}\nu_{zy})G, \tag{2a}$$

$$C_{22}^0 = E_y(1 - \nu_{xz}\nu_{zx})G, \tag{2b}$$

$$C_{33}^0 = E_z(1 - \nu_{xy}\nu_{yx})G, \tag{2c}$$

$$C_{12}^0 = E_x(\nu_{yx} - \nu_{zx}\nu_{zy})G, \tag{2d}$$

$$C_{23}^0 = E_y(\nu_{zy} - \nu_{xy}\nu_{zx})G, \tag{2e}$$

$$C_{13}^0 = E_x(\nu_{zx} - \nu_{yx}\nu_{zy})G, \tag{2f}$$

$$C_{44}^0 = G_{xy}, \tag{2g}$$

$$C_{55}^0 = G_{yz}, \tag{2h}$$

$$C_{66}^0 = G_{xz}, \tag{2i}$$

$$G = 1/(1 - \nu_{xy}\nu_{yx} - \nu_{yz}\nu_{zy} - \nu_{xz}\nu_{zx} - 2\nu_{yx}\nu_{zy}\nu_{xz}). \tag{2j}$$

Here,  $E$  is young’s modulus,  $G$  is shear modulus, and  $\nu$  is Poisson’s ratio.

When the damage has initiated and occurred, the damage elastic constants  $C_{ij}$  are used, which is calculated with the equations given below.

$$C_{11} = (1 - d_f)C_{11}^0, \tag{3a}$$

$$C_{22} = (1 - d_f)(1 - d_m)C_{22}^0, \tag{3b}$$

$$C_{33} = (1 - d_f)(1 - d_m)C_{33}^0, \tag{3c}$$

$$C_{12} = (1 - d_f)(1 - d_m)C_{12}^0, \tag{3d}$$

$$C_{23} = (1 - d_f)(1 - d_m)C_{23}^0, \tag{3e}$$

$$C_{13} = (1 - d_f)(1 - d_m)C_{13}^0, \tag{3f}$$

$$C_{44} = (1 - d_f)(1 - s_{mt}d_{mt})(1 - s_{mc}d_{mc})C_{44}^0, \tag{3g}$$

$$C_{55} = (1 - d_f)(1 - s_{mt}d_{mt})(1 - s_{mc}d_{mc})C_{55}^0, \tag{3h}$$

$$C_{66} = (1 - d_f)(1 - s_{mt}d_{mt})(1 - s_{mc}d_{mc})C_{66}^0. \tag{3i}$$

The factors mentioned in the above equations  $s_{mt}$  and  $s_{mc}$  are used to control the shear stiffness caused by tensile and compressive failure in the matrix, respectively. ABAQUS/Explicit [14] recommends  $s_{mt} = 0.99$  and  $s_{mc} = 0.5$ .

The global fiber and matrix damage variables are as follows:

$$d_f = 1 - (1 - d_{ft})(1 - d_{fc}), \tag{4a}$$

$$d_m = 1 - (1 - d_{mt})(1 - d_{mc}), \tag{4b}$$

where  $d_{ft}$  and  $d_{fc}$  are the damage variables associated with fiber tension and compression failure modes.  $d_{mt}$  and  $d_{mc}$  are the damage variables associated with matrix tension and compression failure modes.

### 3.5 HASHIN failure criteria

The four basic modes of failure occurs in composite structure are matrix cracking, fiber-matrix shearing, fiber failure, and delamination failure [14, 15]. These failure modes strongly depend on ply orientation, loading direction, and geometrical properties of the laminate.

Though many failure criteria are available, HASHIN damage criteria are only capable of evaluating the different modes of failure of the laminate. Hence, the constitutive damage model of the composite laminate used in this analysis is 3D Hashin’s theory.

AUTODESK HELIUS PFA 2016 plug-in is used to include the material properties of the composite laminate, Hashin failure criterion, damage initiation, and damage evolution criteria to the 3D FE model. This plug-in is used for incorporating any one of the selected VUMAT subroutine failure models [15] (Max stress, Max strain, Hashin, Puck, Tsai-Hill, Tsai-Wu, Christensen, LaRC02, etc.). The damage initiation is controlled by the 3D Hashin criteria and damage evolution is based on stiffness degradation factor of 0.1 and  $1E^{-6}$  for matrix and fiber, respectively [15].

The Hashin criterion is capable of evaluating the four different modes of failure for the composite material. The four modes are: tensile fiber failure, compressive fiber failure, tensile matrix failure, and compressive matrix failure [15, 17] which are mentioned by the Hashin equations (5)–(8):

$$\text{Fiber tension } (\sigma_{11} > 0) : \left(\frac{\sigma_{11}}{X_t}\right)^2 + \frac{1}{S_{12}^2}(\sigma_{12}^2 + \sigma_{31}^2) \leq 1, \tag{5}$$

$$\text{Fiber compression } (\sigma_{11} \leq 0) : \left(\frac{\sigma_{11}}{X_c}\right)^2 \leq 1, \tag{6}$$



Matrix tension

$$(\sigma_{22} + \sigma_{33} > 0) : \frac{1}{Y_t^2} (\sigma_{22} + \sigma_{33})^2 + \frac{1}{S_{23}^2} (\sigma_{23}^2 - \sigma_{22}\sigma_{33}) + \frac{1}{S_{12}^2} (\sigma_{12}^2 + \sigma_{31}^2) \leq 1, \quad (7)$$

Matrix compression ( $\sigma_{22} + \sigma_{33} \leq 0$ )

$$: \frac{1}{Y_c} \left[ \left( \frac{Y_c}{2S_{23}} \right)^2 - 1 \right] (\sigma_{22} + \sigma_{33}) + \frac{1}{4S_{23}^2} (\sigma_{22} + \sigma_{33})^2 + \frac{1}{S_{23}^2} (\sigma_{23}^2 - \sigma_{22}\sigma_{33}) + \frac{1}{S_{12}^2} (\sigma_{12}^2 + \sigma_{31}^2) \leq 1. \quad (8)$$

In the above 3D Hashin failure criteria equations:  $X_t$  is the tensile failure strength in fiber direction.  $X_c$  is the compressive failure strength in fiber direction.  $Y_t$  is the tensile failure strength in direction 2 (transverse direction to fiber direction).  $Y_c$  is the compressive failure strength in direction 2 (transverse direction to fiber direction).  $S_{12}$  is the failure shear strength in 1–2 plane.  $S_{23}$  is the failure shear strength in 2–3 plane.  $\sigma$  is the Stress.

### 3.6 Boundary conditions and loading

The boundary conditions for the FE model is applied by considering the real-time situations of the actual milling process, the four sides of the workpiece were fixed (clamped) and arrested for all six degrees of freedom (Encastre:  $U1 = U2 = U3 = UR1 = UR2 = UR3 = 0$ ). The end mill cutter is constrained in  $Y$  and  $Z$  directions, and it is allowed to move along the  $X$  axis (Feed) and rotate along the  $Z$  axis (Spindle speed) only ( $U2 = U3 = UR1 = UR2 = 0$ ). A reference point is created at the tool tip; a translation (feed rate) and rotational velocity (Spindle speed) were applied. The cutting parameters were applied to the FE model as per the details mentioned in Table 1.

## 4 Results and discussion

### 4.1 Cutting force

The cutting force is an important factor which determines the chip morphology and the failure mode of the laminate, which may be predicted with the help of FE simulation tools [7]. The high degree of fluctuation (as shown in Fig. 3, 4, and 5) in the cutting force signal is observed while milling GFRP laminate. This is due to the fiber reinforcement and its orientation in the unidirectional GFRP laminate [7, 18].

Experimental and FEA results show the max cutting force ( $F_x$ ,  $F_y$ ) which decreases with the increase of the cutting speed (m/min). Max cutting force obtained is  $F_{x-} = 32$  N,  $F_y = 31$  N at  $V_c = 10.99$  m/min, and feed rate  $f = 150$  mm/min. The cutting force during the slot milling operation is maximum, at lower feed rates and at lower cutting speeds. Whereas at higher cutting speeds and feed, the cutting force is comparatively in minimum range as shown in Fig. 6 and 7. Moreover, it shows the correlation of the cutting forces obtained from FE and experimental results. These results are harmonious with a deviation of only 10–15% and it also matches with the literature [7, 9]. These results confirm the quality of the developed 3D FE model in predicting the cutting forces during the slot milling process.

Figures 3, 4 show the comparison of cutting force profiles ( $F_x$  and  $F_y$ ) obtained from the experimental and FE model. These figures show a good agreement between FE and experimental results. The FE model as well as experimental results show negative value of cutting forces in  $x$  direction ( $F_x$ ) for every cycle of tool rotation. This is because the chip thickness is theoretically equal to zero at  $180^\circ$  tool rotation. Moreover, the small difference in the comparison of the experimental and FE thrust force profiles is due to the tool run-out during the milling process [21]. Figure 5 shows how the cutting forces  $F_x$  and  $F_y$  vary with respect to the tool rotation angle for one teeth.

### 4.2 Working stress

The results obtained from the FE simulation reveal the maximum stressed regions of GFRP laminate. The maximum stress during material removal & chip formation is 174.6 MPa, which is greater than the ultimate shear strength of the material. Shearing is predominant in the milling process due to the sliding action of the tool with the workpiece. Figure 8 shows the development of maximum shear stress during cutting action and chip formation.

### 4.3 Modes of failure predicted from FE results

The machining simulation recorded from the FEA results exposes the different modes of failure in the GFRP laminate as mentioned in Sect. 3.5. The Solution-Dependent state Variable (SDV) plots were captured to understand the modes of failure effectively.

The plot SDV1 shows the damage state of the UD-GFRP laminate; since it has reached the value of 2.0, it reveals the complete failure of the matrix.

SDV2 results predict the matrix failure index; in this case, the epoxy matrix material has reached its ultimate strength, which is interpreted from the maximum value of 1.0. The SDV3 reveals the fiber failure index. The plot

**Fig. 3** Comparison between experimental and FE model values of cutting force ( $F_x$ ) in slot milling of GFRP laminate at  $V_c = 10.99$  m/min,  $N = 350$  rpm, feed rate = 150 mm/min, and depth of cut = 1 mm

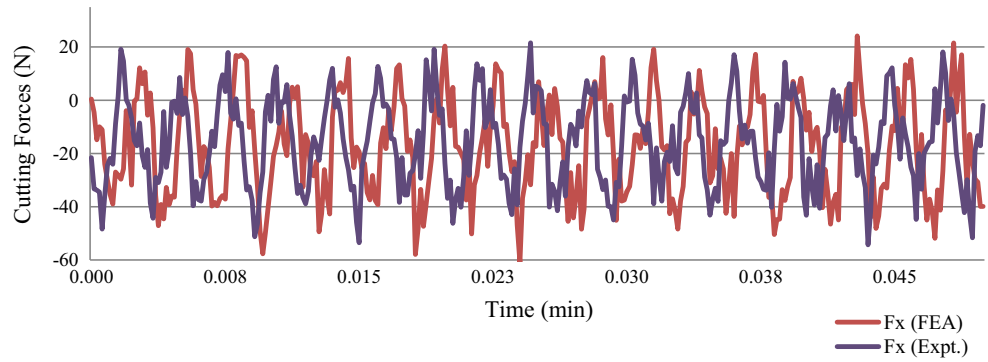


**Fig. 4** Comparison between experimental and FE model values of cutting force ( $F_y$ ) in slot milling of GFRP laminate at  $V_c = 10.99$  m/min,  $N = 350$  rpm, and feed rate = 150 mm/min

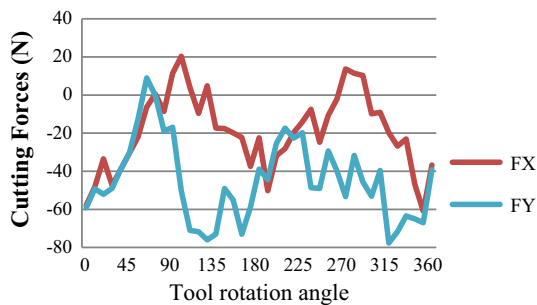
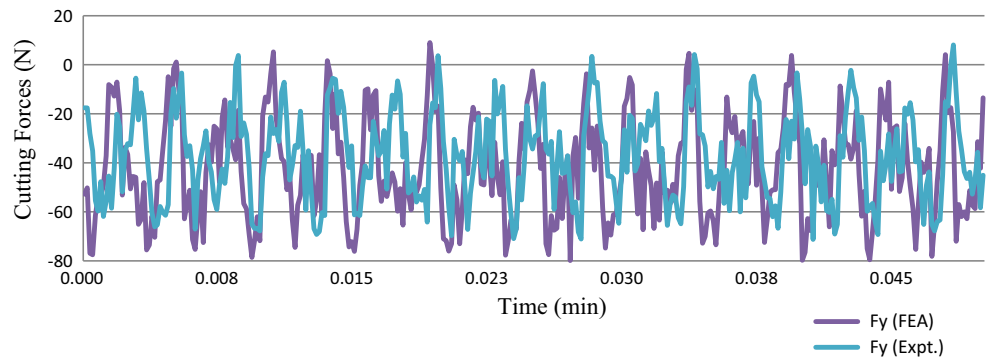


**Fig. 5** Cutting force profile vs tool rotation angle

obtained from FE results shows the maximum value of 0.9989 which means that the working stress in the fiber has reached 99.89% of its ultimate strength.

SDV4 plot shows whether the material undergoes compressive/tensile failure. During the tool rotation from

180° to 90° clockwise, the chip is machined by up-milling process. Whereas, when the tool rotates from 90° to 0° clockwise, it is a down-milling process (shown in Fig. 9a).

The SDV4 plot captures the very important failure mode of the fiber. Compressive fiber failure takes place during the first 90° of tool rotation after the tool engagement, which is ensured by the value  $-0.875$ . Tensile fiber failure is observed during the next 90° of tool rotation, which is also visualised from the SDV4 plot (shown in Fig. 9b).

#### 4.4 Chip formation process in FEA

The chips obtained from the FE simulation results are tiny and curled. The chip curls along the rake face of the end mill cutter and it breaks due to the lack of ductility of the GFRP material, which is the main reason for getting curled chips [7, 9, 10], as shown in Fig. 10.

**Fig. 6** Feed rate and cutting speed vs max cutting force ( $F_x$ )

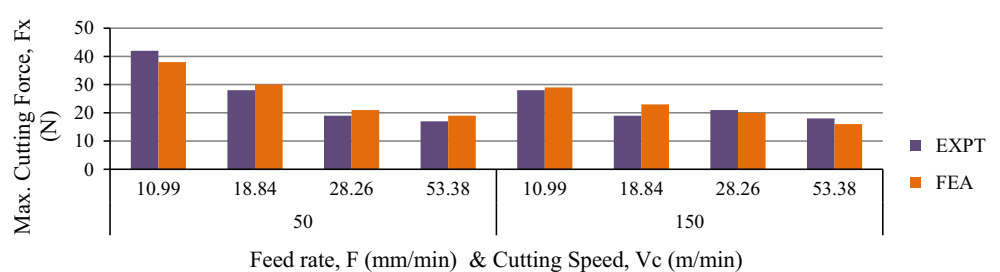
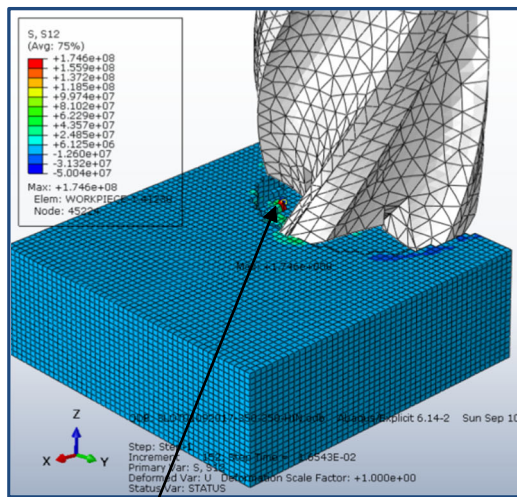
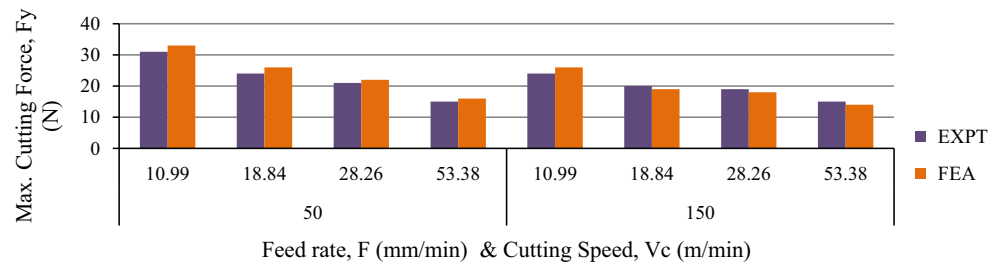
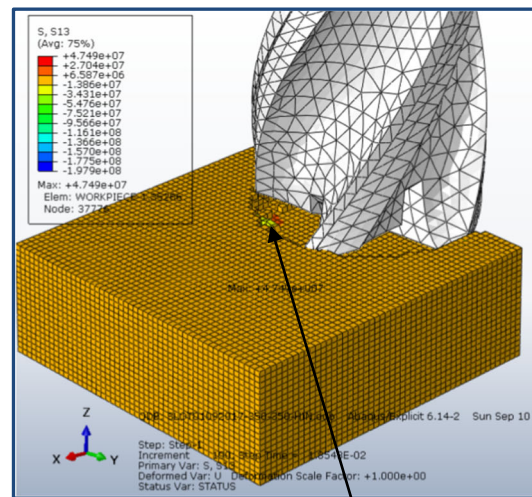


**Fig. 7** Feed rate and cutting speed vs max cutting force ( $F_y$ )



Max shear stress (S12) of 174.6 MPa.

(a)



Max shear stress (S13) of 47.49 MPa.

(b)

**Fig. 8** a Shear stress plot (S12); b) shear stress plot (S13) from FEA results

Moreover, the chip obtained from FE simulation and from experimental results is in good agreement (shown in Figs. 10, 11, 12, 13). This is evident that the developed FE model is also good in predicting the chip characteristics very effectively.

#### 4.5 Chip characteristics

It is very important to investigate the chip formation, chip characteristics to understand the machinability, and the possibilities of machining defects in the GFRP laminate. The chip characteristics mainly depend on the cutting speed and feed rate. Hence, the influence of the cutting parameters on chip morphology must be studied to machine defect-free slots and to understand the slot milling process effectively. The chips obtained from the experimental tests are white in colour.

Figure 11 reveals that the failure of the laminate is mainly due to delamination and fiber pullout is also more, which is observed at the lower feed rate of 50 mm/min and

spindle speeds,  $N < 1000$  rpm. At lower cutting speed, the epoxy matrix produces chips comparatively larger in size.

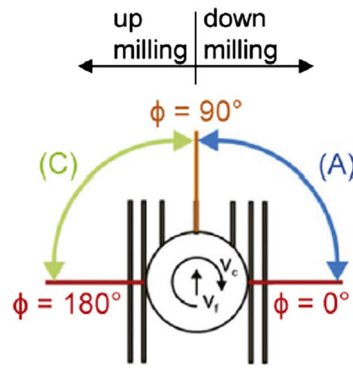
At higher spindle speeds,  $N > 1000$  rpm and 150 mm/min feed rate, the delamination and fiber pullout is comparatively minimum and the chip tends to curl along the rake face of the tool. The smaller segmented chips are obtained in this case due to the development of higher strain rate in the epoxy matrix.

However, due to the lack of ductility in GFRP composites [7, 9], the chip does not deform further, which results in discontinuous and tiny curled chips with fiber pull-out, as shown in Fig. 12. The chip photographs make us to understand that the chip formation is mainly due to shearing action of the tool and the chip is released due to the bending and buckling of fiber and matrix. Plastic deformation is not observed for any of the machining conditions [9].

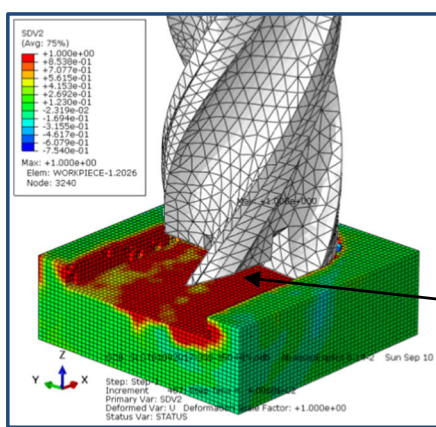
Figures 12, 13 shows the magnified image (20 $\times$ ) of the chips obtained from experimental and FEA results, respectively, at the machining conditions  $V_c = 10.99$  m/



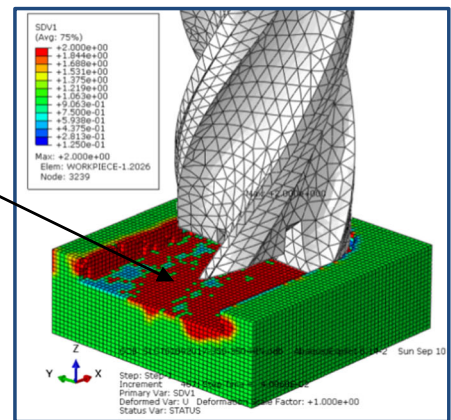
**Fibre orientation angle  $\theta=0^\circ$**



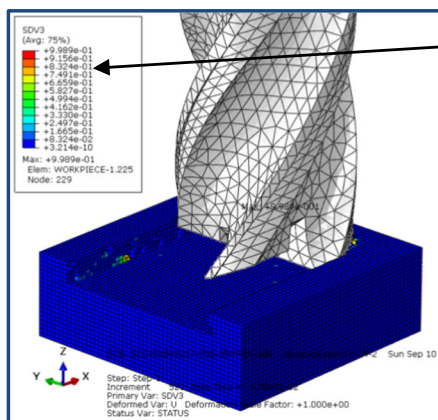
(a)



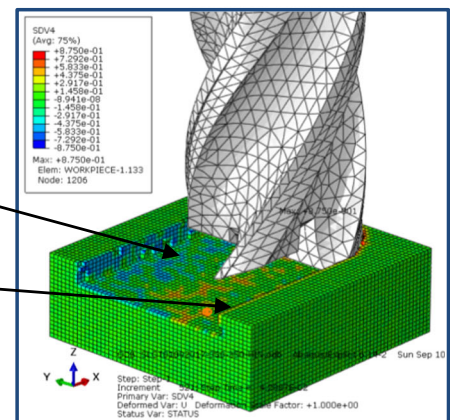
Matrix Failure Status (SDV2)



Laminate Failure Status (SDV1)



Fiber Failure Status (SDV3)  
(99.89 %)



Compressive Fiber Failure

Tensile Fiber Failure

(b)

**Fig. 9 a** Milling process with respect to fiber orientation. **b** State-dependent variables (SDV) plots

min,  $N = 350$  rpm, feed rate = 150 mm/min. The chips obtained for these machining conditions are not definite [7, 9]. The chips obtained are of different shapes like, tiny curled, flakes, delaminated stripped pieces with fibers,

sheared pieces with fiber and matrix, etc. Comparing Figs. 12 and 13, it is found that the chips obtained from experiment and FE results are similar in shape and size (curled chips and delaminated strips). This is evident that

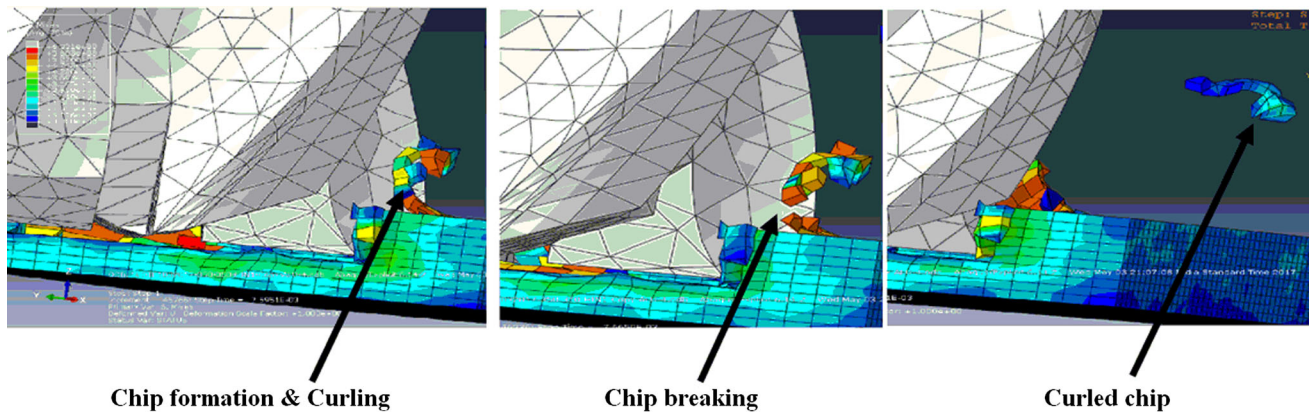


Fig. 10 Chip formation process in FEA simulation

Feed rate/ Spindle Speed	350 (rpm)	660 (rpm)	900 (rpm)	1700 (rpm)
50 (mm/min)				
150 (mm/min)				

Fig. 11 Chip characteristics of GFRP laminate under different cutting conditions

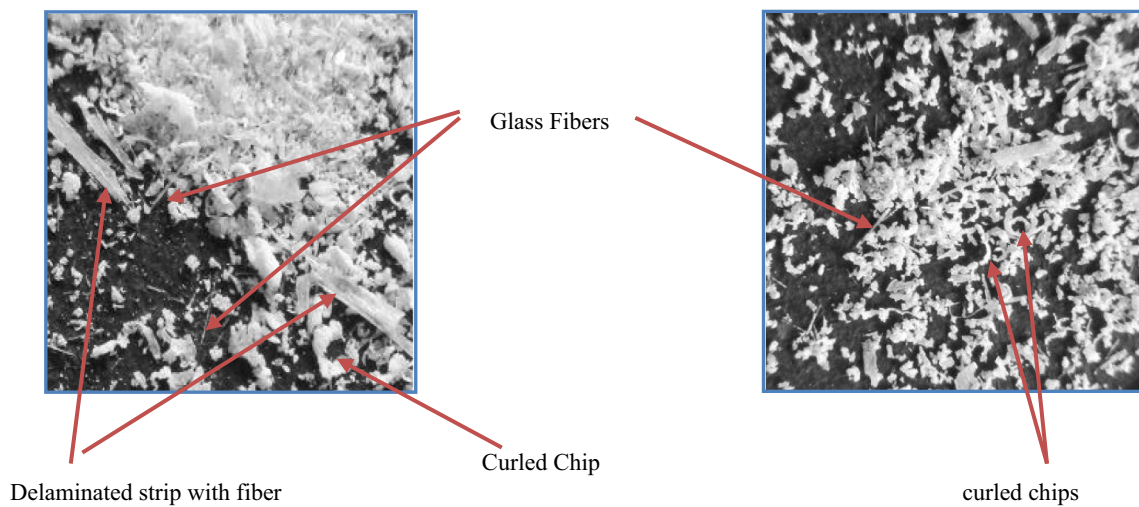
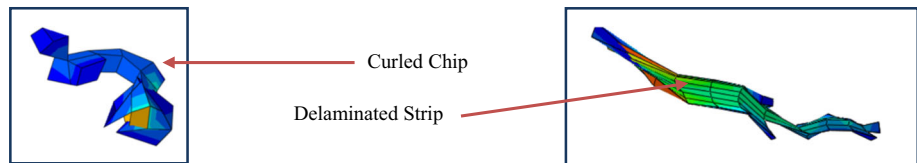


Fig. 12 Experimental chip characteristics at  $N = 1700$  rpm and at the feed rate: a 50 mm/min and b 150 mm/min



**Fig. 13** Image of the milled chip (chip images from FEA results) at  $V_c = 10.99$  m/min,  $N = 350$  rpm, and feed rate = 150 mm/min



the FE model is capable of simulating and predicting the chip characteristics very effectively.

#### 4.6 Microstructure of the chips

The scanning electron microscopy (SEM) technique was used to analyze the chip characteristics and microscopic study of the chips for the different machining parameters. SEM images of chips were taken on JEOL make Scanning Electron Microscope Equipment (JSM-6610LV).

It is mandatory for the SEM specimens to be conductive, but the GFRP composite is a non-conductive material, and hence, the SEM specimens were prepared by coating the milled chips with platinum, using JFC—1600 Auto fine coater machine, as shown in Fig. 14.

SEM images of the milled GFRP chips are shown in Figs. 15, 16, and 17. The chip microstructure images obtained from SEM reveals, the GFRP laminate undergoes different modes of failures, such as fiber pullout, fiber fracture, matrix cracking, plastic deformation of matrix and delamination, loosening of matrix due to the increase in

stress, shearing of fiber, and debonding of fiber and matrix during the slot milling process [7, 18]. The SEM images of the milled chips are also in accordance with the literature [7, 18].

The SEM photographs of the milled chips shown in Figs. 15, 17 disclose the way which the glass fiber behaves during milling process. The glass fiber produce chips with partial bending and cracking which results in fiber pullout which is predominant. Since glass is an amorphous material the fracture of the fiber is smooth and brittle in nature [7].

#### 5 Conclusions

The 3D FE model is developed to simulate the slot milling process in a GFRP laminate. The FEM results are correlated with experimental results and they are found to be in good agreement. The outcome of this research work is the validated 3D FE Model which not only simulates the slot milling process, but also predicts the chip formation, chip

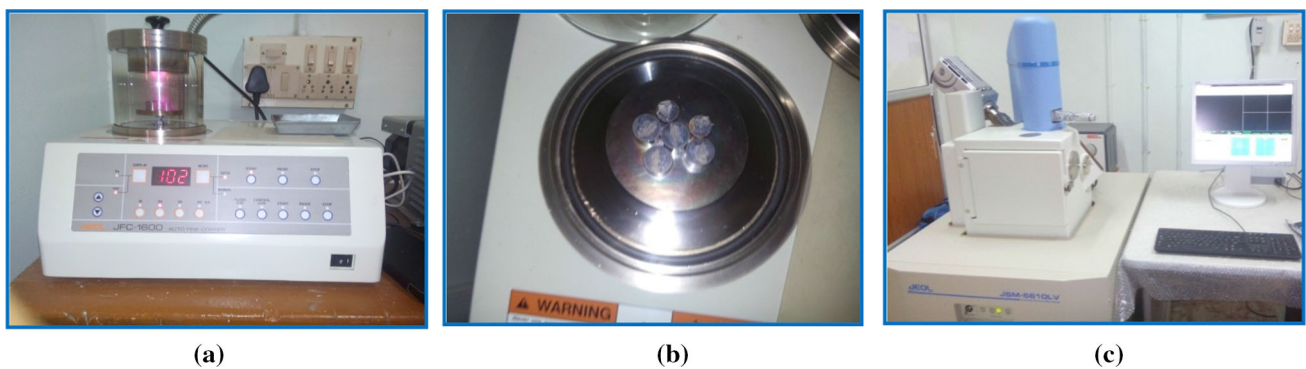


**Fig. 14** a Coating machine, b SEM sample preparation, and c SEM equipment with data acquisition

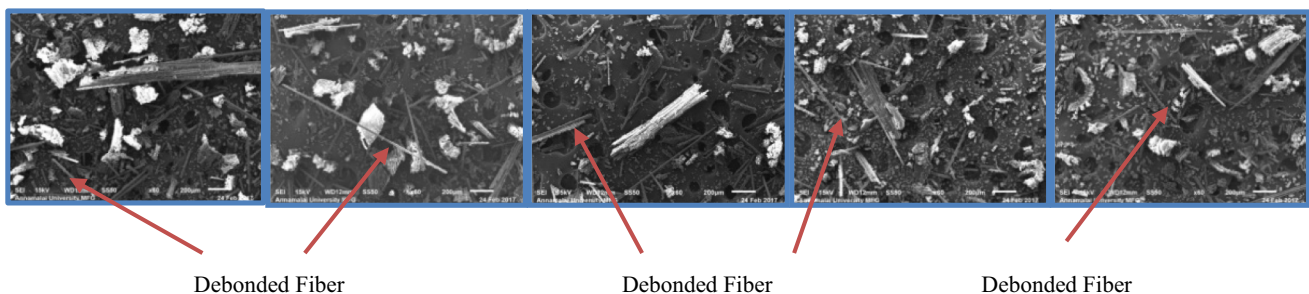


**Fig. 15** SEM micrographs of chips from slot milling of UD—GFRP laminate for different machining parameters

**Fig. 16** SEM micrographs of slot milled chip with various modes of failure

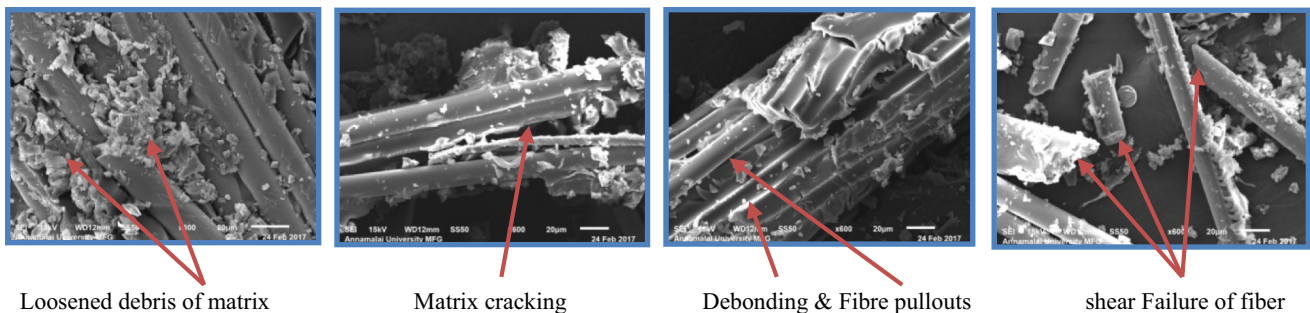
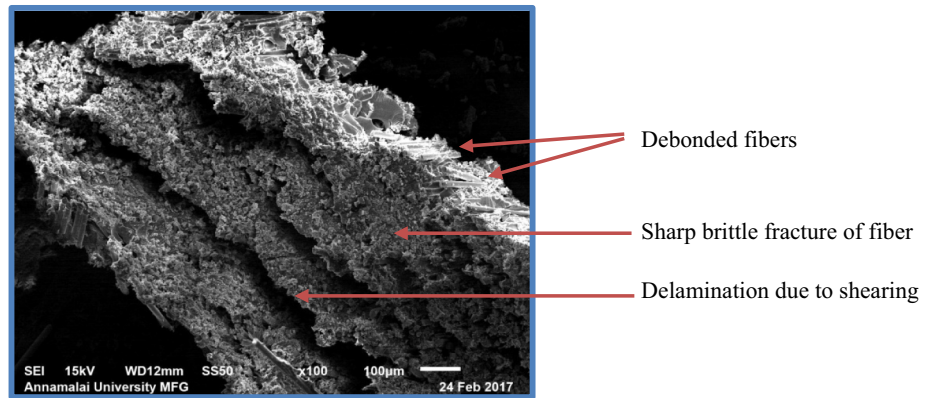


**Fig. 17** Close-up images of fractured glass fibers for different machining parameters (refer Table 2)

characteristics, stress, cutting forces, and the possibilities of various modes of laminate failure. Moreover, this FE Model predicts the influences of the cutting parameter settings on milling process and it also reduces/cuts the cost involved in experimentation and testing. Numerous trial simulations can be carried out with the help of this 3D FE model with different cutting parameters which helps the industries to select a suitable cutting parameter setting.

- The cutting force results predicted by the FE model are correlated with the experimental results. The variation amongst them ranged between 10 and 15% only. Therefore, it is evident that the developed FE model is quite efficient to predict the cutting force signals.
- The stress plot obtained from the FE reports shows the shear stress (S12) during the material removal is around 175 MPa, which is higher than the ultimate shear strength of the material. This facilitates the shearing action during the metal cutting, chip formation, and removal process.
- The feed rate and spindle speed influences chip formation for the slot milling operation. Moreover, due to the lack of ductility in GFRP composites, the chip deforms only a little, which results in discontinuous and tiny curled chips. At lower cutting speeds, delamination and fiber pullout are predominant. The chips obtained from FE simulation result are found to be similar in shape to the experimental results.

- The chip morphological studies reveal the different modes of laminate failures such as matrix cracking, loosening of matrix due to the increase in stress, shearing of fiber, debonding of fiber and matrix, and fiber pullout.
- The different state-dependent variables (SDVs) plots from FE results reveal the failure status and the factor of safety of the fiber and matrix.

## 6 Acknowledgements

The authors are indebted to AICTE (All India Council for Technical Education) for the financial support in this work. The authors thank the Department of Mechanical Engineering, SSN College of Engineering for providing the Laboratory and Testing Facility.

## References

1. Alajji R, Lasri L, Bouayad A (2015) 3D finite element modelling of chip formation and induced damage in machining of fiber reinforced composites. *Am J Eng Res* 4(7):123–132
2. Phadnis VA, Roy A, Silberschmidt VV (2012) Finite element analysis of drilling in carbon fiber reinforced polymer composites. IOP Publishing. *J Phys Conf Ser* 382(2012):012014

3. Dhawan V, Debnath K (2016) Prediction of forces during drilling of composite laminates using artificial neural network: a new approach. *FME Transact* 44(1):36–42. <https://doi.org/10.5937/fmet1601036D>
4. Soldani X, Santiuste C, Muñoz-Sánchez A, Miguélez M (2011) Influence of tool geometry and numerical parameters when modeling orthogonal cutting of LFRP composites. *Compos A Appl Sci Manuf* 42(9):1205–1216
5. Oğuz ÇOLAK, Talha SUNAR (2016) Cutting forces and 3D surface analysis of CFRP milling with PCD cutting tools. *Elsevier Proc CIRP* 45:75–78
6. Ghafarizadeh S, Chatelain J-F, Lebrun G (2016) Finite element analysis of surface milling of carbon fiber-reinforced composites. *Int J Adv Manuf Technol* 87:399–409. <https://doi.org/10.1007/s00170-016-8482>
7. Sheikh-Ahmad JY (2009) *Machining of polymer composites*. Springer
8. Giasin K, Ayyar-Soberanis S, French T, Padnis V (2016) 3D finite element modelling of cutting forces in drilling fibre Metal laminates and experimental hole quality analysis. *Appl Compos Mater*. <https://doi.org/10.1007/s10443-016-9517-0>
9. Azmi AI (2013) Chip formation studies in machining fibre reinforced polymer composites. *Int J Mater Prod Technol* 46(1):32–46
10. Lasri L, Nouari M, el Mansori M (2009) Modelling of chip separation in machining unidirectional FRP composites by stiffness degradation concept. *Compos Sci Technol* 69(5):684–692
11. He YL, Liu YL, Gao JG (2015) Macro and micro models of milling of carbon fiber reinforced plastics using fem. *International Conference on Artificial Intelligence and Industrial Engineering (AIIE 2015)*. Atlantis Press. <https://doi.org/10.2991/aiie-15.2015.151>
12. Isbilir O, Ghassemieh E (2013) Three-dimensional numerical modelling of drilling of carbon fiber-reinforced plastic composites. *J Compos Mater*. <https://doi.org/10.1177/0021998313484947>
13. Chakladar ND, Pal SK, Mandal P (2012) Drilling of woven glass fiber-reinforced plastic-an experimental and finite element study. *Int J Adv Manuf Technol* 58:267–278
14. Simulia D (2014) *Abaqus 6.14 User's manual*. Dassault systems, Providence, RI. <http://130.149.89.49:2080/v6.14/index.html>
15. Autodesk (2016) *Autodesk Heliux PFA 2016/HELP*, Autodesk Knowledge Network. <http://help.autodesk.com/view/ACMPAN/2016/ENU/?guid=GUID-05546EDB-D1D1-4D0F-B5D6-4C1B9FCB281C>
16. CATIA V5R14 (2014) *User Manual*, Dassault systems. Providence, RI. [http://www.catia.com.pl/tutorial/z2/part\\_design.pdf](http://www.catia.com.pl/tutorial/z2/part_design.pdf)
17. Hashin Z (1980) Failure criteria for unidirectional fiber composites. *J Appl Mech* 47:329–334
18. Krishnamurthy R, Santhanakrishnan G, Malhotra SK (1992) *Machining of polymeric composites*. In: *Proceedings of the Machining of Composites Materials Symposium*. ASM Materials Week. Chicago, Illinois, pp 139–148
19. Vijay Sekar KS, Pradeep Kumar M (2011) Finite element simulations of Ti6Al4V titanium alloy machining to assess material model parameters of the Johnson-Cook constitutive equation. *J Braz Soc Mech Sci Eng* 33(2):203–211
20. Phadnis VA, Makhdam F, Roy A, Silberschmidt VV (2013) Drilling in carbon/epoxy composites: experimental investigations and finite element implementation. *Compos Part A* 47:41–51
21. Li C, Lai X, Li H, Ni J (2007) Modeling of three-dimensional cutting forces in micro-end-milling. *J Micromech Microeng* 17(4):67